Nguyen, D. H., Lowenberg , M. H., & Neild, S. A. (2021). Effect of Actuator Saturation on Pilot-Induced Oscillation: a Nonlinear Bifurcation Analysis. *Journal of Guidance, Control, and Dynamics*, *44*(5), 1018-1026. https://doi.org/10.2514/1.G005840

Effect of Actuator Saturation on Pilot-Induced Oscillation: a Nonlinear Bifurcation Analysis

Duc H. Nguyen,[1] Mark H. Lowenberg[2], and Simon A. Neild[3]

Department of Aerospace Engineering, University of Bristol, Bristol, BS8 1TR

Nomenclature

A = forcing amplitude (deg)

K_P = proportional pilot gain

OLOP = open-loop onset point

PIO = pilot-induced oscillation

q = pitch rate (deg/s)

T = time delay constant (s)

t = time (s)

u = stick input (deg)

x = general state vector

η = elevator/elevon deflection (deg)

λ = general input vector

ω = forcing frequency (rad/s)

θ = pitch angle (deg)

Subscript

dem = demanded

[1] PhD student, Department of Aerospace Engineering, Student Member AIAA.
[2] Professor of Flight Dynamics, Department of Aerospace Engineering, Senior Member AIAA.
[3] Professor of Nonlinear Structural Dynamics, Department of Aerospace Engineering.

I. Introduction

Actuator saturation has been identified as the leading cause of many high-profile pilot-induced oscillations (PIO) and limit-cycle oscillations. The problem stretches back to the early days of fly-by-wire technology with the X-15, which encountered both PIO [1, 2] and a fatal limit-cycle oscillation [3] caused by rate saturation in the horizontal stabilizers. Due to its highly nonlinear nature, rate saturation can still be overlooked by many existing linear-based handling qualities criteria [4], which consider the X-15 to meet level-1 requirements and not PIO-prone [2]. The more recent crashes of the highly unstable Gripen fighter jet in 1993 and 1999 were also attributed to rate saturation in its elevon, which was overloaded by intensive pitch and roll control demands during the accident [5]. In all these cases, the impact of rate limiting was not predicted before the accidents, and subsequent investigations only employed quasi-nonlinear methods (e.g. describing functions [2, 3, 5]), to supplement the original linear-based analysis. Therefore, there is a need to develop a more powerful toolbox for the industry that can not only handle nonlinearities efficiently, but also is presented in a familiar manner to facilitate its adoption by the practicing engineers.

In recent years, bifurcation analysis and numerical continuation have proven to be a powerful tool for nonlinear flight dynamics analysis. Thanks to its ability to fully characterize many nonlinear phenomena in both open- [6-8] and closed-loop applications [9-11], the method has gained recognition in the research community as well as in the industry. Nevertheless, there is still little (if any) research on the effect of actuator saturation on flight dynamics using bifurcation analysis apart from a brief mention in [12]. This is a promising research topic, as previous studies have demonstrated the potential of bifurcation analysis on providing a complete picture of the various nonlinear attractors that govern the dynamics of the aircraft. The method has also recently been expanded to generate the 'nonlinear Bode plot' of a harmonically-forced flight dynamics model – a technique we refer to as 'frequency-domain bifurcation analysis' or 'nonlinear frequency response' [13]. There are two advantages to this approach: 1) the Bode plot is a familiar tool for many practicing engineers, which would facilitate the adoption of the method in the industry, and 2) frequency analysis involves calculating the non-stationary solutions of the system, which means that the effect of actuator saturation can be directly observed. Since the latter capability is not available in conventional bifurcation analysis of equilibrium solutions (i.e., the approach employed in [6-11]), frequency-domain bifurcation analysis is especially suitable for studying the effect of actuator saturation on flight dynamics.

This note illustrates how both conventional and frequency-domain bifurcation analysis can be exploited to evaluate the contribution of actuator rate and position saturations on pilot-induced oscillations. We first demonstrate how the

methods can be directly applied to existing PIO criteria for linear airframes in Sections II and III. Then, Section IV examines the Space Shuttle's PIO incident – an example of a complex closed-loop system – which uncovers additional insights that cannot be reflected using existing PIO criteria or analysis methods. The ultimate goal is to provide a useful tool for the research community and the industry. All results presented were calculated using numerical continuation [14] via the Dynamical Systems Toolbox [15] – a MATLAB/Simulink implementation of the numerical continuation software AUTO [16].

II. Limit Cycle Analysis

For the first study, we employ conventional bifurcation analysis to repeat the analysis in [2], which studies the formation of limit cycles in the X-15 at landing condition. For a system written in the form $\dot{\boldsymbol{x}} = f(\boldsymbol{x}, \boldsymbol{\lambda})$, where $\boldsymbol{x}$ is the state vector and $\boldsymbol{\lambda}$ is the input vector, conventional bifurcation analysis solves for $\dot{\boldsymbol{x}} = \boldsymbol{0}$ to generate a map of equilibrium and periodic solutions of each state in $\boldsymbol{x}$ when one of the input parameters in $\boldsymbol{\lambda}$ is varied. This map is referred to as a 'bifurcation diagram', which also provides information on the solutions' stability. To illustrate the technique using a simple linear example, consider the pilot-vehicle system shown in Fig. 1 consisting of a proportional gain representing the pilot and the pitch-angle-to-elevator transfer function of the X-15 airframe at landing condition [2]. It should be noted that in [2], the gain in equation (1) has already been adjusted for 0 dB crossing at –110° phase in the open-loop frequency response, so a pilot gain of K_P = 1 in this example refers to the baseline condition.

$$\frac{\theta(s)}{\eta(s)} = \frac{3.476(s+0.883)(s+0.0292)}{(s^2 + 0.038s + 0.01)(s^2 + 1.684s + 5.29)} \tag{1}$$

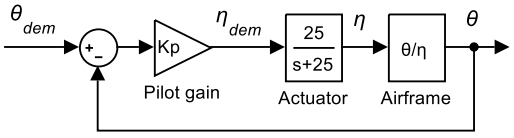

Fig. 1 Block diagram: X-15 with a synchorous pilot model.

The linear pilot-vehicle system under consideration becomes unstable when K_P exceeds the 17 dB gain margin obtained from the open-loop frequency response, corresponding to K_P = 7.1. We can make the same prediction using bifurcation analysis by trimming the aircraft at the origin using zero reference input (θ_{dem} = 0°), then setting the pilot gain as the continuation parameter (i.e., making K_P the varying control parameter in $\boldsymbol{\lambda}$). Fig. 2a shows the resulting

bifurcation diagram of the pitch angle θ as a function of K_P, which is a map of the system's equilibrium solutions as K_P increases. Due to the zero reference input, the equilibrium solution is at the origin regardless of the K_P value, as expected. However, there is a change of stability from stable to unstable at K_P = 7.1 – the same value predicted by the linear gain margin. This change of stability is caused by a Hopf bifurcation that gives rise to a limit cycle. As all components are linear, the limit cycle is divergent whenever K_P exceeds 7.1.

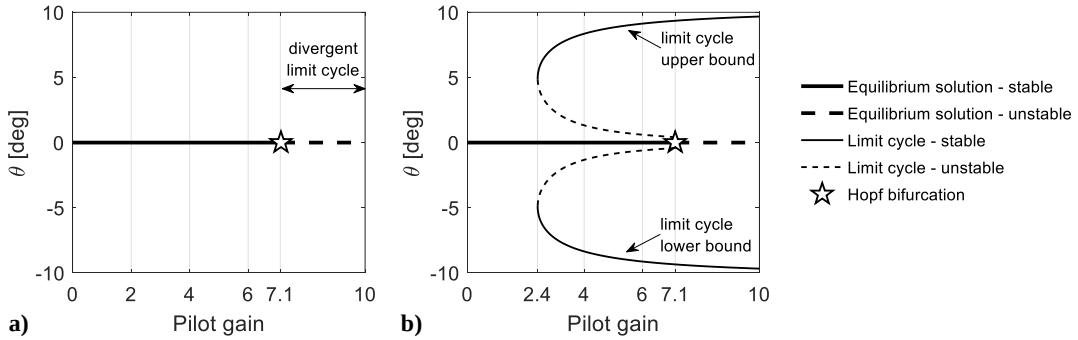

Fig. 2 Unforced bifurcation diagram of the a) linear and b) rate-limited X-15 pilot-vehicle system.

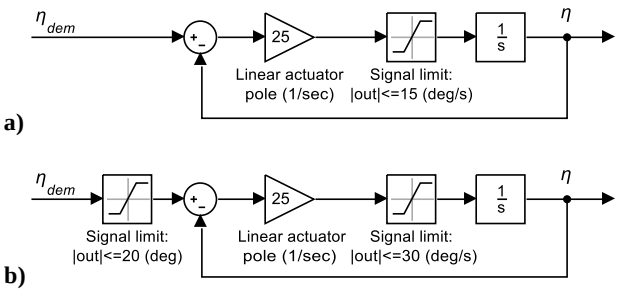

Fig. 3 X-15 nonlinear actuator block diagram: a) rate limit only and b) both rate and position limits.

We now repeat the analysis but with the actuator rate limited at 15 deg/s. Based on [2, 17], rate saturation is modelled by limiting the magnitude of the signal just before the integrator block as shown in Fig. 3a. This results in the nonlinear rate-limited bifurcation diagram shown in Fig. 2b. Although the Hopf bifurcation still occurs at K_P = 7.1, the limit cycle is now bounded and coexists with the equilibrium solutions in the region $2.4 \leq K_P \leq 7.1$. In other words, the Hopf bifurcation is now subcritical. This is a very undesirable behaviour because a limit cycle now exists for K_P as low as 2.4 and that in the region $2.4 \leq K_P \leq 7.1$, the response can jump from the equilibrium branch to the limit cycle without warning if the perturbation is sufficiently large. We verify this in Fig. 4, which shows the time simulation of the aircraft subjected to a small perturbation at the 5s mark and a larger one at the 20s mark. Unlike the

first case, the second disturbance is large enough to send the aircraft into the stable limit cycle. The coexistence of the limit cycle and the equilibrium solutions also leads to jump phenomena. Fig. 5 shows the rate-limited bifurcation diagram with data from another time simulation superimposed in green. The simulation started in a limit cycle at a high pilot gain, which was then slowly reduced to 0. It can be seen that as the pilot gain reduces past the Hopf bifurcation at K_P = 7.1, the response remains in the limit cycle until K_P drops below 2.4, where the oscillation ceases and the response converges to the equilibrium solution again. For further reference, mathematical discussions of limit cycles in a similar setting can be found in [18, 19]; the latter presents a case in which the limit cycle can been measured experimentally.

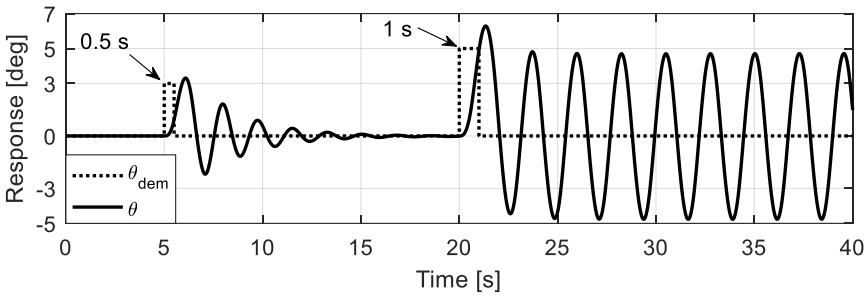

Fig. 4 X-15 response to two elevator impulse inputs – K_P = 2.41.

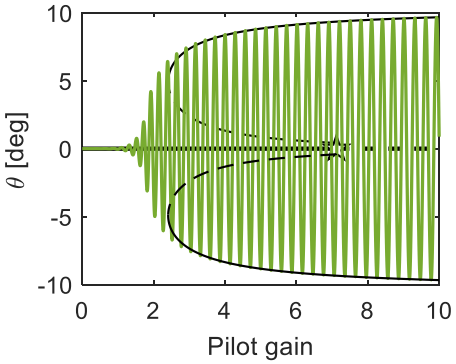

Fig. 5 X-15 response to jump phenomenon due to slowly decreasing K_P.

One might assume that a better actuator with higher travel rate will improve the situation by raising the stability margin. This is not necessary the case, however. Fig. 6 shows the rate-limited bifurcation diagram of the pitch angle θ and the elevon angle η for a range of rate limits. It can be seen that despite the faster actuator, the limit cycle onset is still at K_P = 2.4. The oscillation amplitude, on the other hand, increases with the travel rate, i.e. making the situation worse. However, simualtions show that a larger peturbation is needed to enter the limit cycle when the actuator travel

rate increases. In practice, this means the input peturbation required can be so large that it might exceed the deflection limit of the elevator and therefore has no chance of occuring. To demonstrate, we impose a deflection limit of 20 deg and a rate limit of 30 deg/s on the actuator using the scheme shown in Fig. 3b. The ensuing bifurcation diagram is also shown in Fig. 6 (marked as '30 deg/s + travel limit'). It is clear from Fig. 6b that the deflection limit has confined the elevator state η within the 20 deg boundary, which results in a reduced limit cycle amplitude of θ in Fig. 6a compared to when deflection limit is not implemented. The value of Fig. 6b is that it demonstrates the susceptibility of an aircraft to position saturation. While time series simulations with perturbation inputs can also indicate this, such a technique is reliant on giving the system the appropriate level of perturbation at the appropriate time, which can be very difficult to predict. Additionally, it does not yield information on the parameter dependence of the dynamics governing the behavior observed.

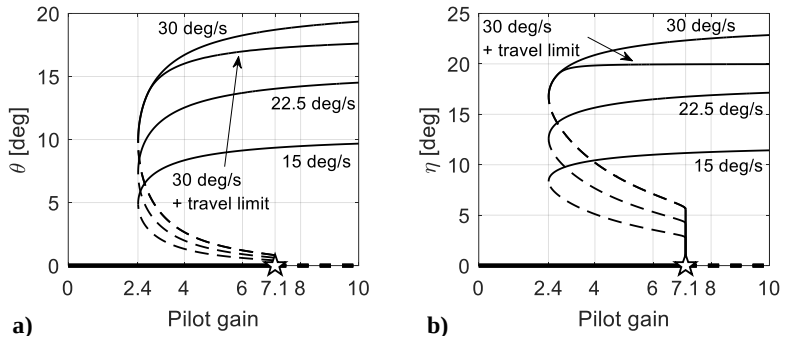

Fig. 6 X-15 bifurcation diagrams of the a) pitch angle and b) elevator states with different actuator rate limits.

The same analysis using the inverse describing function technique was also presented in [20] and it was noted that that while the method can predict existence of limit cycles, it does not provide an indication of the aircraft's susceptibility to entering the oscillation, and hence the PIO. This limitation is also reflected in Fig. 6 by the fact that both the limit cycle onset at K_P = 2.4 and the Hopf bifurcation at K_P = 7.1 are unaffected by the maximum actuator rate. A frequency-domain analysis can overcome this issue, which is discussed in the next section.

III. Nonlinear Open-Loop Frequency Response

We now employ frequency-domain bifurcation analysis to generate the open-loop frequency response under the original 15 deg/s rate saturation and no deflection constraint. In this instance, the demanded pitch angle takes the form $\theta_{dem} = A\sin(\omega t)$, where A and ω are the forcing amplitude and frequency in deg and rad/s, respectively. Numerical

continuation requires the system to be time-invariant (no t on the right-hand side of the state equations). Therefore, it is necessary to convert the forcing term $\theta_{dem} = A\sin(\omega t)$ into the required form using equations (3-5). It can be shown that $x_6 = \sin(\omega t)$ and $x_7 = \cos(\omega t)$, essentially making them 'dummy states' to provide a harmonic forcing. The model is now effectively a 7th-order system described by equations (2-5), which consists of $[x_1, x_2, \dots, x_4]$ to describe the airframe transfer function in equation (1), x_η for the actuator state, and the harmonic oscillator $[x_6, x_7]$. Nonlinear frequency analysis can be now executed by setting ω as the continuation parameter. Although the harmonic oscillator had been employed in some earlier works [7, 12, 21], a full nonlinear Bode plot with both gain and phase information has not employed in a flight dynamics context until recently [13].

$$\left[\dot{x}_1, \dot{x}_2, \dots, \dot{x}_4, \dot{x}_\eta\right]^T = \boldsymbol{f}(x_1, x_2, \dots, x_4, x_\eta, \theta_{dem}) \tag{2}$$

$$\theta_{dem} = Ax_6 \tag{3}$$

$$\dot{x}_6 = x_6 + \omega x_7 - x_6(x_6^2 + x_7^2) \tag{4}$$

$$\dot{x}_7 = x_7 - \omega x_6 - x_7(x_6^2 + x_7^2) \tag{5}$$

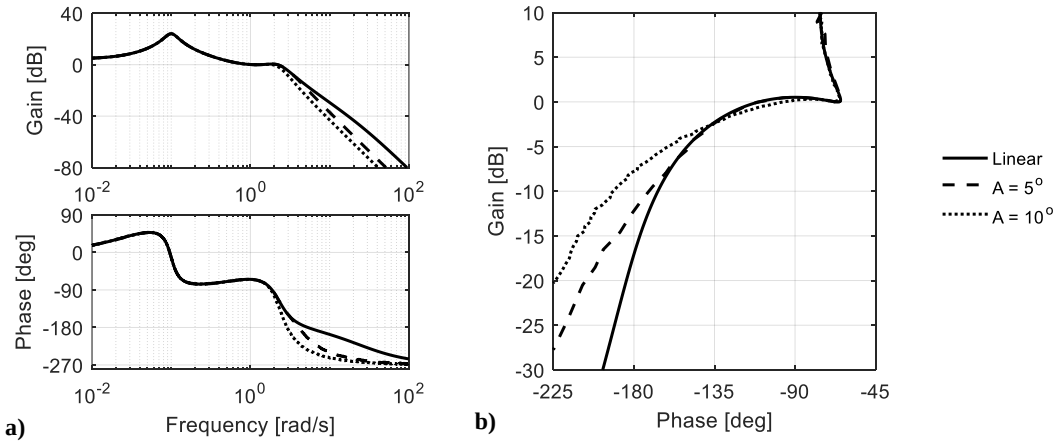

Fig. 7 X-15 open-loop θ-to-η_{dem} a) Bode and b) Nichols charts under different forcing amplitudes A: linear and rate-limited at 15 deg/s.

Fig. 7 compares the θ-to-η_{dem} frequency responses of the ideal and the rate-limited open-loop aircraft with no pilot. The 17 dB gain margin mentioned previously can be seen in the linear response. For the rate-limited case, the frequency response is dependent on both the forcing frequency and amplitude – a characteristic of nonlinear systems. Increasing the forcing amplitude will significantly reduce gain margin and lead to a lower roll-off frequency because

the actuator cannot keep up with the reference signal even at low frequencies. It was shown in [2] that using the linear frequency-domain criteria, the aircraft meets level 1 handling qualities and is not PIO-susceptible. However, due to the large influence of the actuator rate limiting, the assumptions involved in applying those linear criteria are no longer valid due to the strong mismatch between the linear and nonlinear frequency responses. If we ignore the assumption of linear dynamics and employ nonlinear frequency response analysis, then Fig. 7b shows that the rate-limited responses violate the Gibson PIO criterion.

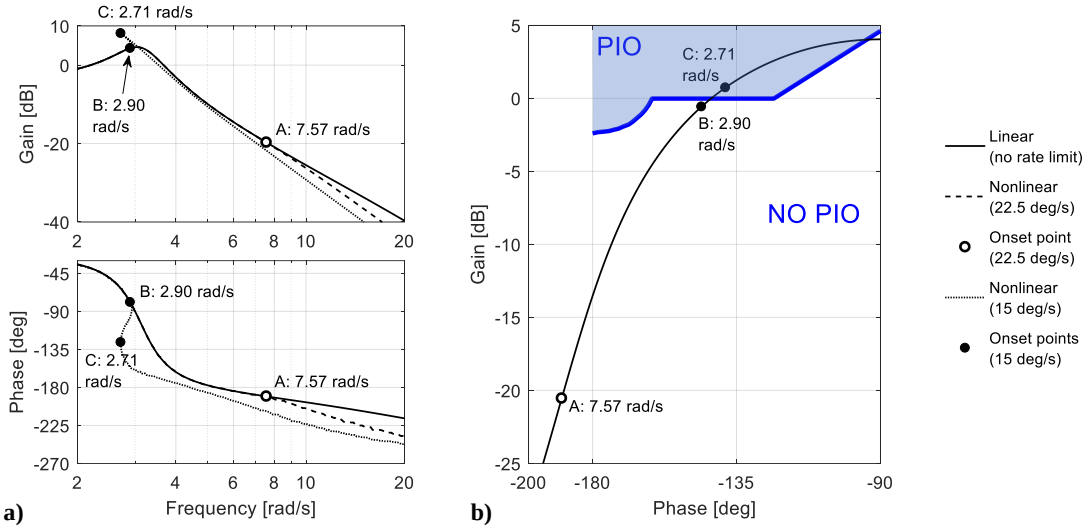

Fig. 8 X-15 a) closed-loop and b) open-loop θ-to-θ_{dem} frequency responses at [K_P, A] = [1.5, 2].

Using the rate-limited frequency response, we can now employ other frequency-domain Category II PIO criteria such as the open-loop onset point (OLOP) boundary [20, 22] in our analysis. The applications of OLOP criterion to various aircraft including the X-15, has previously been discussed in [4] using other techniques such as describing functions. In this section, the procedure using numerical continuation is explained. We chose a pilot gain of K_P = 1.5, which is well below the limit-cycle onset value in Fig. 6 and may therefore be listed as not PIO-prone using limit-cycle analysis in Section II. The first step is to determine the onset frequency; this is the lowest frequency at which rate limiting first becomes active in the closed-loop system. Fig. 8a compares the closed-loop Bode plots of the linear and nonlinear frequency responses. The onset points are marked as black and white circles for two different levels of rate limiting. Then, plot the onset frequencies on the open-loop Nichols chart (Fig. 8b). The following observations can be made:

- At 22.5 deg/s rate limiting, the onset point A matches the prediction made based on the procedure described in [20]. Point A lies well outside the blue boundary in Fig. 8b, indicating that the aircraft is safe from PIO.

- At 15 deg/s rate limiting, there are two possible onset points: point B is the one obtained using the method in [20], which lies very close to the PIO boundary in Fig. 8b. The OLOP criterion therefore suggests that the aircraft may be on the verge of being PIO prone and requires further examination. Nonlinear frequency response analysis reveals that poor handling qualities is indeed a problem, as a small increase in the forcing frequency beyond point B results in a cliff-like jump in phase lag. Additionally, a second onset point labelled C is also detected at a lower frequency, which falls within the OLOP boundary and provides further evidence of a PIO-prone platform. Time simulation verifies that rate limiting can occur above 2.71 rad/s (and below 2.90 rad/s) if the aircraft is given a large enough perturbation.

The behaviour observed in the 15 deg/s case is caused by a pair of fold bifurcations and explains the jump resonance mentioned in [20, 22]. This highly nonlinear phenomenon and its implications are discussed in the next section and in the appendix; the latter provides an example where jump resonance can be easily observed in a simple second-order system. For our current discussion, nonlinear frequency analysis has revealed that rate limiting onset can occur in more than one way (at more than one frequency), depending on which side of the 'cliff' the pilot is on.

It has been shown that rate limiting can lead to highly undesirable dynamics even in a very simple linear system. In both the limit cycle and the frequency response analyses, rate saturation causes the aircraft's responses to differ significantly from the linear predictions. Bifurcation analysis, on the other hand, not only accurately predicts the dynamics, but can also be directly employed on existing PIO criteria. In the next section, the influence of actuator saturation will be further studied in a complex closed-loop system to investigate the flying qualities cliff phenomenon.

IV. Nonlinear Closed-Loop Frequency Response: Analysis of the Space Shuttle PIO

A. Description

We now investigate the PIO incident encountered on the Space Shuttle Enterprise, which also occurred during landing flare on the final flight (FF-5) of the approach and landing test program (ALT). The Enterprise was built for pilot training and comes without an engine and heat shield [23]. Its typical mission started on the back of a Boeing 747, where the Shuttle was released at altitude to glide back to the landing site. Regarding the PIO, investigations by NASA concluded that a combination of rate limiting and excessive time delay led to the degraded handling quality of the Space Shuttle at landing [24]. Subsequent efforts to prevent further PIO included extensive pilot training [23] and the introduction of a new PIO-suppression filter onboard the operational Space Shuttles, which reduces the input gain

at certain known problematic frequencies [25]. In this section, we examine the closed-loop frequency response of the unmodified Enterprise at landing configuration – the one in which flight FF-5 suffered the PIO. The model used for analysis is based on the NASA TM 81366 report [24].

Fig. 9 shows the block diagram of the Shuttle's linearised pitch rate control system with the airframe transfer function described by equation (6). The nonlinear elements (not shown in Fig. 9) are the actuator's rate and travel limits. Input shaping is not considered in this study as only the actuator nonlinearities are of interest. In the original NASA report, rate and travel limits were implemented using the scheme described by Fig. 10a, which involves taking the derivative of the elevon demand signal η_{dem}. Bifurcation analysis requires the components to be written in autonomous ordinary differential equations form, so it is impractical to use the derivative signal of η_{dem}. To address this, the scheme shown in Fig. 10b is used to model rate and travel saturations (similar to the one used for the X-15 above). We have verified that the simulated responses of these two configurations are very similar. Nevertheless, all time simulations presented in this section were generated using the original scheme in Fig. 10a to ensure the validity of the results. For the time delay block e^{-Ts}, a Padé 3rd-order approximation is used to ensure that the only nonlinear elements in the analysis are still actuator rate and deflection saturations.

$$\frac{q(s)}{\eta(s)} = \frac{-1.3s(s+0.648)(s+0.0349)}{(s+0.887)(s-0.1)(s^2+0.189s+0.238143)} \tag{6}$$

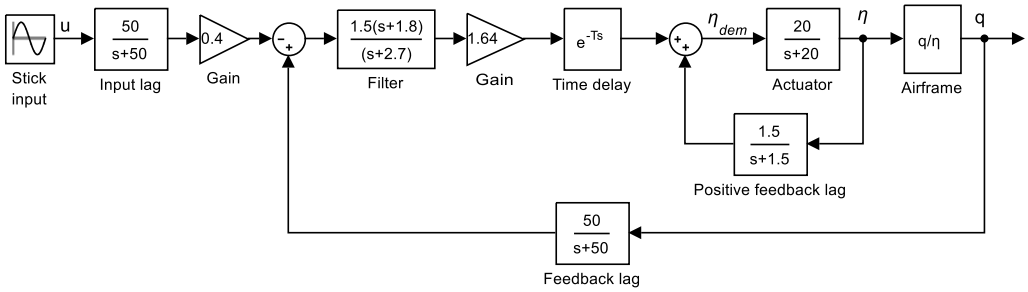

Fig. 9 Linear representation of the Space Shuttle's pitch rate control system (based on [24]).

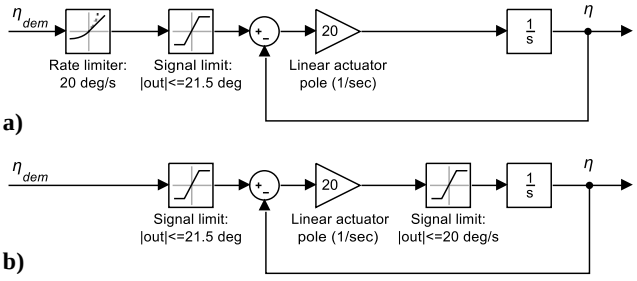

Fig. 10 Space Shuttle rate and travel limit implementations for a) time simulation and b) bifurcation analysis.

B. Frequency and amplitude responses

The original NASA report [24] considers time delays T between 0.1 and 0.4 s. For the first analysis, the worst-case scenario of T = 0.4 s is considered. Fig. 11a compares the linear and nonlinear frequency responses. Due to the nonlinearity introduced by rate limiting, the nonlinear responses are functions of both forcing frequency ω and forcing amplitude A. More specifically, larger A reduces the roll-off frequency due to the actuator not travelling fast enough to follow the input signal. In extreme cases like at A = 15°, a pair of fold bifurcations at 1.19 and 1.58 rad/s is detected. Each fold bifurcation reverses the direction of the solution branch in the gain plot, causing a change of stability from stable to unstable (and vice versa). As a consequence, the resonance curve leans to the left and leads to a region of two stable solutions between these two fold bifurcations. Moreover, the stable solutions in this range have a phase difference of almost 180°. One might attribute this highly nonlinear behaviour to the large forcing amplitude, which requires the elevon to travel at a higher speed at lower frequency. However, it is shown that reducing the forcing amplitude to 5° does little to improve the situation as the fold bifurcation and the large phase jump are still observed.

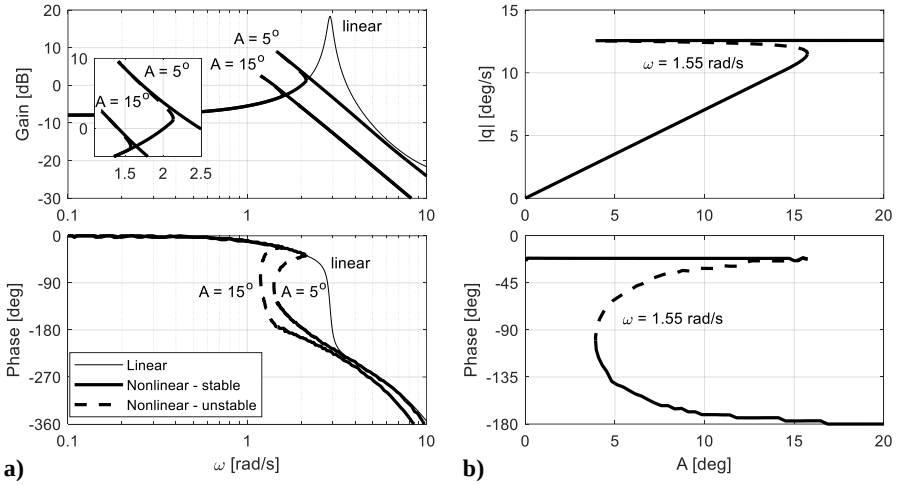

Fig. 11 Space Shuttle closed-loop q-to-u a) frequency and b) amplitude responses – T = 0.4 s.

An advantage of numerical continuation methods is that the dependency on the forcing amplitude can be directly assessed. By fixing ω while allowing A to vary, the system's gain and phase responses as a function of only the forcing amplitude can be generated as shown Fig. 11b, in which the forcing frequency is fixed at 1.55 rad/s. As before, a region of multiple solutions (two stable and one unstable) arising from a pair of fold bifurcations is detected for 3.9° $\leq A \leq$ 15.7°, which has dangerous implications. Fig. 12 shows the simulated response with fixed amplitude at 15° and a frequency of 1.55 rad/s, which lies inside the region where two stable responses exist. Before the perturbation at the

159 s mark, the motion corresponds to the in-phase solution with a phase lag of roughly 22°. The perturbation causes a violent transition to the out-of-phase solution and eventually converges to the stable response with a 177° phase lag. This transition resembles the 'flying qualities cliff' phenomenon, which is described in [2] as a *"sudden and dramatic incremental shift in the phase lag, equivalent to the sudden insertion of a significant incremental time delay into the loop, initiated by only a slight change in pilot input command."* Studies have identified actuator rate limiting as the main cause of the flying qualities cliff, making modern high-performance fly-by-wire aircraft especially vulnerable [26]. Despite its potential consequence, the issue has not been thoroughly analysed or documented due to its highly nonlinear and elusive nature. As shown in the time simulation in Fig. 12, the transition to the out-of-phase motion can be sudden and violent, which catches the pilot off guard and contributes to PIO. This also makes it extremely hard to predict when the pilot might encounter the cliff and to replicate the phenomenon using time simulation unless the exact parameters are known beforehand. On the other hand, we have shown that nonlinear frequency response analysis can circumvent this challenge, and Fig. 11 is the first successful attempt at characterising the flying qualities cliff using bifurcation analysis and numerical continuation.

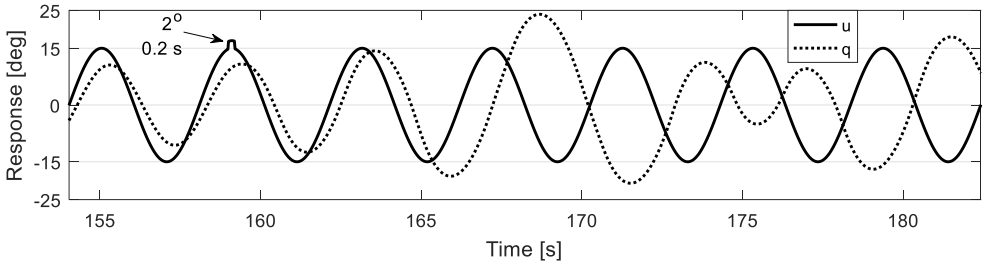

Fig. 12 Space Shuttle simulated response to an input perturbation for [T, A, ω] = [0.4, 15, 1.55].

With the PIO fully developed, the pilot may attempt to stop the out-of-phase motion by reducing the forcing amplitude. However, the fold bifurcation at A = 3.9° in Fig. 11b will impede the recovery process. As the response will always follow the nearest stable solution, once the motion lands on the out-of-phase region at A = 15°, reducing A sees no change in the pitch rate amplitude along with a very small reduction in phase lag all the way down to A = 3.9°, at which point, a sudden jump back to the low-amplitude and in-phase response is observed. We verify this by forcing the aircraft at 1.55 rad/s but with the forcing amplitude reducing linearly at a rate of 0.1 deg/s, shown in Fig. 13. It can be seen that before A passes 3.9°, there is no reduction in the pitch rate response amplitude despite a constantly reducing A. In practical terms, this behavior suggests that the only way to recover the aircraft in this

situation is to release the stick, which is hardly an option when the PIO is fully developed with the aircraft already close to the ground at landing, potentially while also at a dangerous attitude.

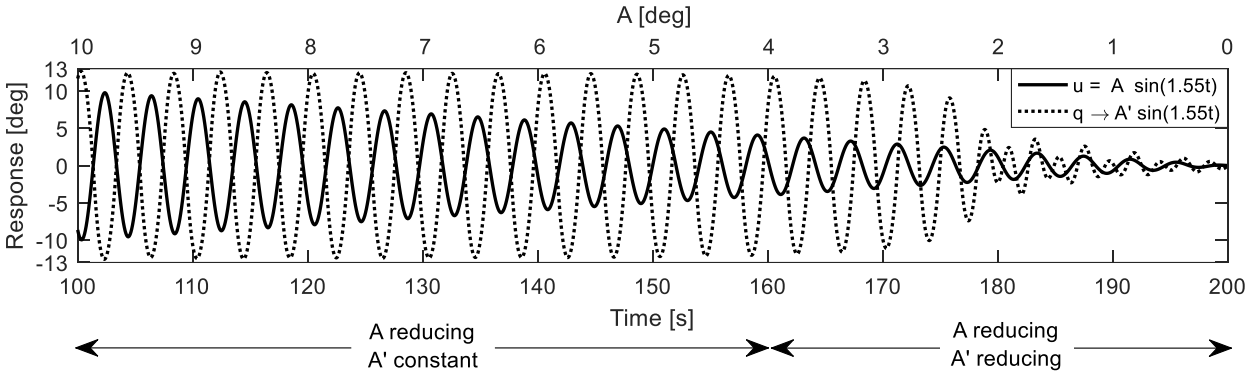

Fig. 13 Space Shuttle simulated response with a linearly reducing forcing amplitude.

C. Effects of time delay

Fig. 14 shows the frequency responses at $A = 15^{o}$ for a range of time delay constant T. Although reducing T from 0.4 s to 0.1 s improves the situation by narrowing the frequency separation between the fold bifurcations and reducing the magnitude of the phase jump, the fold bifurcations still exist. In fact, they only disappear by reducing the time delay further. This suggests that both rate limiting and time delay contribute to the formation of the fold bifurcations and consequently the phase jump that caused the PIO, but not time delay alone since the Padé approximation is linear and therefore cannot create the fold bifurcations. Although the original NASA report also drew similar conclusions through experience, frequency-domain bifurcation analysis can systematically identify the precise mechanism of the

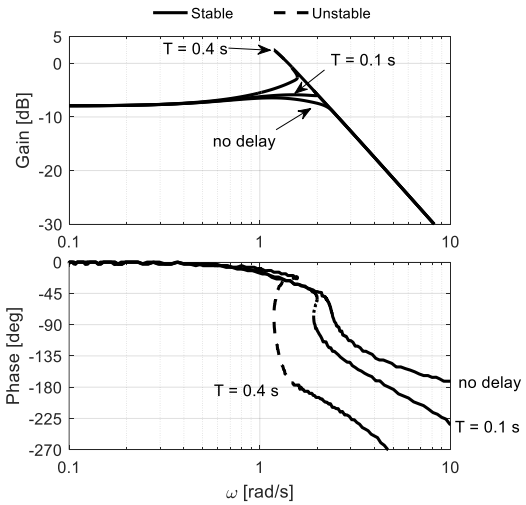

Fig. 14 Space Shuttle rate-limited frequency responses for a range of time delay levels at $A = 15^{o}$.

flying qualities cliff that contributed to the PIO experienced on the Enterprise. We validate the prediction of multiple stable solutions at T = 0.1 s, A = 15°, and ω = 1.96 rad/s using time simulation with different initial conditions. Fig. 15 confirms that there are indeed two possible responses for the same forcing input: one with 45° and one with 95° phase lag, and that the elevon is rate-saturated in both instances.

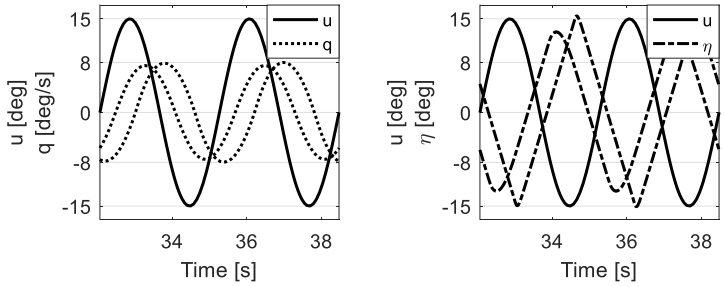

Fig. 15 Space Shuttle pitch rate responses from two different simulations with different initial conditions. $[T, A, \omega] = [0.1, 15, 1.96]$.

D. Detecting position saturation

Finally, we demonstrate another advantage of continuation methods: the frequency response of an element inside a closed-loop can be examined. Of particular interest in this example is that of the elevon state η. Its frequency responses at T = 0.4 s for three different forcing amplitudes are shown in Fig. 16. It can be seen that for A = 6.5° and above, the resonance peak is flattened at η = 21.5°, which is the elevon travel limit. We verify this by forcing the Space Shuttle at A = 6.5° with a chirp signal that linearly decreases the forcing frequency at a rate of -0.005 rad/s^2. Its pitch rate response in Fig. 17a shows the jump phenomenon as discussed previously. The elevon response between 1.35 and 1.25 rad/s is shown in Fig. 17b, and is clearly position-saturated as predicted (in addition to being rate-saturated).

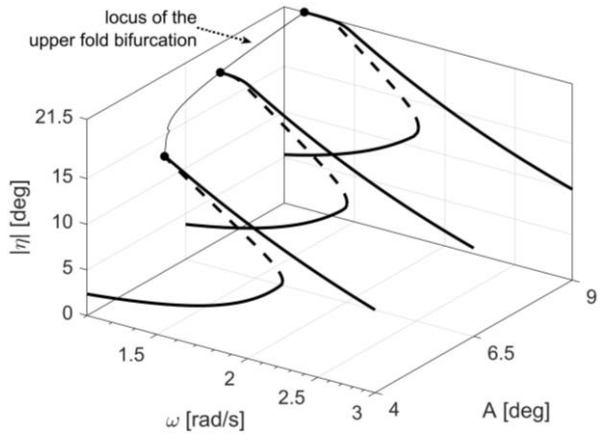

Fig. 16 Frequency responses of the Space Shuttle's elevon state η at T = 0.4 s.

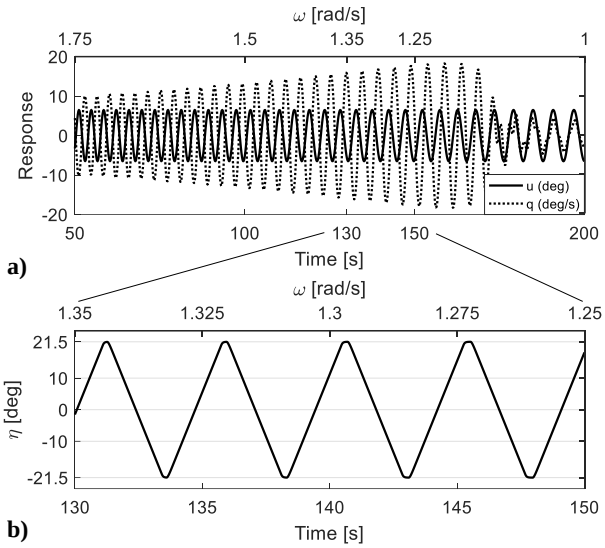

Fig. 17 Space Shuttle a) pitch rate and b) elevon response to a chirp signal for [T, A] = [0.4, 6.5].

The Space Shuttle's susceptibility to position saturation can be analyzed by examining the movement of the upper fold bifurcation as the forcing amplitude and frequency varies. This locus of the fold bifuraction was calculated using two-parameter continuation method and is shown as the thin line in Fig. 16, along with its projection onto the A-η plane in Fig. 18. Fig. 18 shows that for T = 0.4 s, the line asymptotes to η = 21.5° from around A = 5°, indicating that pumping the stick beyond 5° amplitude will lead to position saturation. Reducing the time delay constant to 0.3 s sees a significant improvement, and now a forcing amplitude of 12° is required to induce travel saturation. In practice, a margin can be defined to ensure the limit is not reached. The benefit of the two-parameter continuation technique is that it can find the locus of a bifurcation point in the two-parameter space in a single run, which is much more computationally efficient than generating the individual frequency responses as shown in Fig. 16. Additionally, the only way to extract information on position saturation without bifurcation analysis is through time simulation, which is very time-consuming and is essentially 'hit or miss' if the range of susceptible parameters is not known in advance.

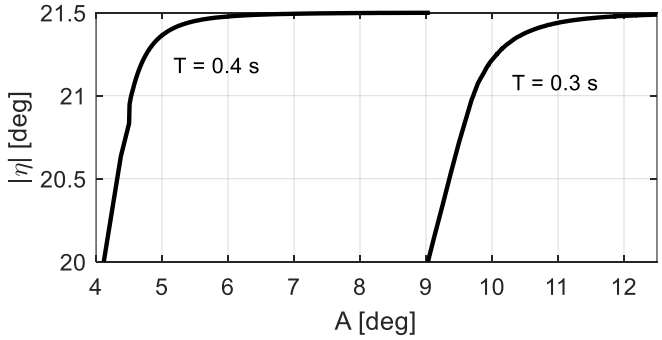

Fig. 18 Two-parameter continuation of the upper fold bifurcation in the A-η plane.

V. Conclusions

In this note, we have proposed the use of both conventional and frequency-domain bifurcation analysis in assessing PIO susceptibility due to rate limiting while also accounting for the contribution of position saturation. Re-examinations of the X-15 illustrates how bifurcation analysis can be directly implemented on existing Category I and II PIO prediction techniques, and the Space Shuttle studies further highlights the method's advantages by explaining the dangerous flying qualities cliff phenomenon, which is very hard to predict and is not reflected in many existing PIO criteria. Comparing to other techniques such as the describing function method, bifurcation analysis offers the following benefits:

1) Systems with multiple nonlinear elements can be analysed.

2) It is not required to know the exact form of the signal going into the nonlinear element. In practice, this means frequency analysis involving a nonlinear controller (such as gain scheduled) or a nonlinear plant can be easily done.

3) In the nonlinear frequency response, both the frequency the amplitude dependencies can be directly assessed.

4) The frequency response of an element inside a closed loop can be examined, as seen from the travel saturation example.

Presenting the results in the form of a nonlinear Bode plot enables the new findings to be viewed by the practising engineers in a familiar context. This further facilitates adoption of the method and makes bifurcation analysis a valuable addition to both the industry and academia. Finally, as nonlinear frequency response involves generating the (non-equilibrium) periodic solutions, there is potential to expand the method to account for other non-stationary phenomena such as unsteady aerodynamics and aeroservoelasticity.

Appendix: Example of Jump Resonance in a Simple Feedback System with Saturation

Jump resonance may be encountered in feedback systems when the error signal is heavily saturated. A simple example is provided here as a potential starting point for further investigations. Consider a second-order actuator model from [27] with a 1200 deg/s^2 accleration limit and no rate saturation. Its schematic block diagram is shown in Fig. 19a, in which the signal limit block has been scaled to compensate for the 21.4 gain in the outer loop. Fig. 19b shows the closed-loop frequency responses for a range of forcing amplitudes A in degrees. Jump resonance appears at

A = 5 and 7°. For low forcing amplitudes like 1°, the actuator is not acceleration-saturated in the frequency range considered, resulting in a linear-like frequency response with a natural frequency of 30 rad/s and damping ratio of 0.7. The jump responance leads to a region of two stable solutions, which can be verified in time simulation (Fig. 20). Increasing or reducing the forcing amplitude beyond the bistable region will lead to a cliff-like jump in phase lag.

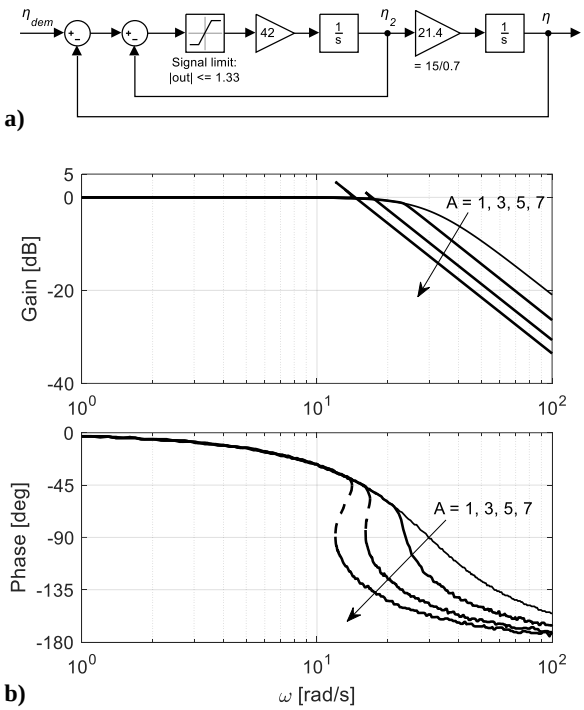

Fig. 19 a) Block diagram and b) closed-loop η-to-η_{dem} frequency responses of a second-order actuator model with 1200 deg/s^2 acceleration limit.

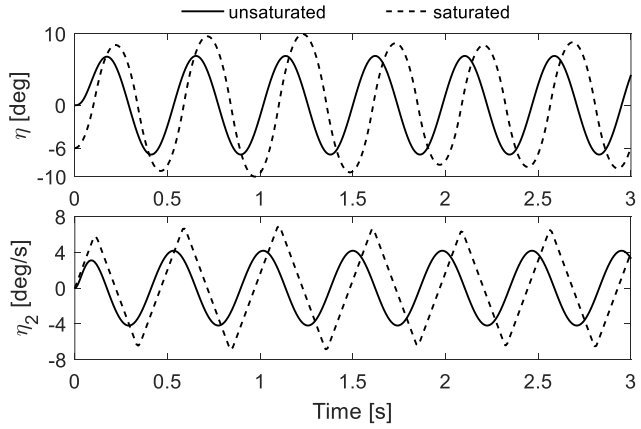

Fig. 20 Simulated responses under the same forcing input [A, ω] = [7, 13] but different initial conditions of η.

Acknowledgement

The first author is partially supported by the University of Bristol's Alumni Grant. We also gratefully acknowledge Mr David H. Klyde at Systems Technology for his valuable suggestions and Dr Etienne B. Coetzee for his help with the DST software.

References

1. Matranga, G. J. "Analysis of the X-15 landing approach and flare characteristics determined from the first 30 flights," *NASA Technical Note D-1057*. National Aeronautics and Space Administration, Flight Research Center, Edwards, CA, 1961.

2. Klyde, D. H., McRuer, D. T., and Myers, T. T. "Pilot-Induced Oscillation Analysis and Prediction with Actuator Rate Limiting", *Journal of Guidance, Control, and Dynamics*, Vol. 20, No. 1, 1997, pp. 81-89. doi: 10.2514/2.3998

3. Orr, J. S., and Dennehy, C. J. "Analysis of the X-15 Flight 3-65-97 Divergent Limit-Cycle Oscillation", *Journal of Aircraft*, Vol. 54, No. 1, 2016, pp. 135-148. doi: 10.2514/1.C033703

4. Annonymous. "Flight Control Design – Best Practices," *RTO Technical Report 29*. NATO, Neuilly-sur-Seine, France, 2000.

5. Rundqwist, L., and Hillgren, R. "Phase compensation of rate limiters in JAS 39 Gripen", *21st Atmospheric Flight Mechanics Conference*, Paper 96-3368-CP, 1996. doi: 10.2514/6.1996-3368

6. Gill, S. J., Lowenberg, M. H., Neild, S. A., Krauskopf, B., Puyou, G., and Coetzee, E. "Upset Dynamics of an Airliner Model: A Nonlinear Bifurcation Analysis", *Journal of Aircraft*, Vol. 50, No. 6, 2013, pp. 1832-1842. doi: 10.2514/1.C032221

7. Gránásy, P., Thomasson, P. G., Sørensen, C. B., and Mosekilde, E. "Non-linear flight dynamics at high angles-of-attack", *The Aeronautical Journal*, Vol. 102, No. 1016, 1998, pp. 337-344. doi: 10.1017/S0001924000027585

8. Goman, M. G., Zagainov, G. I., and Khramtsovsky, A. V. "Application of Bifurcation Methods to Nonlinear Flight Dynamics Problems", *Progress in Aerospace Sciences*, Vol. 33, No. 9-10, 1997, pp. 539-586. doi: 10.1016/S0376-0421(97)00001-8

9. Gill, S. J., Lowenberg, M. H., Neild, S. A., Crespo, L. G., Krauskopf, B., and Puyou, G. "Nonlinear Dynamics of Aircraft Controller Characteristics Outside the Standard Flight Envelope", *Journal of Guidance, Control, and Dynamics*, Vol. 38, No. 12, 2015, pp. 2301-2308. doi: 10.2514/1.G000966

10. Richardson, T., Lowenberg, M., Di Bernardo, M., and Charles, G. "Design of a Gain-Scheduled Flight Control System Using Bifurcation Analysis", *Journal of Guidance, Control, and Dynamics*, Vol. 29, No. 2, 2006, pp. 444-453. doi: 10.2514/1.13902

11. Goman, M. G., and Khramtsovsky, A. V. "Application of continuation and bifurcation methods to the design of control systems", *Philosophical Transactions of the Royal Society of London. Series A: Mathematical, Physical and Engineering Sciences,* Vol. 356, No. 1745, 1998, pp. 2277-2295.
doi: 10.1098/rsta.1998.0274

12. Mehra, R. K., and Prasanth, R. K. "Bifurcation and limit cycle analysis of nonlinear pilot induced oscillations", *23rd Atmospheric Flight Mechanics Conference,* AIAA Paper 98-4249, 1998.
doi: 10.2514/6.1998-4249

13. Nguyen, D. H., Lowenberg, M. H., and Neild, S. A. "Frequency-Domain Bifurcation Analysis of a Nonlinear Flight Dynamics Model", *Journal of Guidance, Control, and Dynamics,* Vol. 44, No. 1, 2020, pp. 138-150.
doi: 10.2514/1.G005197

14. Krauskopf, B., Osinga, H. M., and Galán-Vioque, J., *Numerical continuation methods for dynamical systems: path following and boundary value problems*, Understanding Complex Systems, chapter 1, Springer, Dordrecht, 2007.
doi: 10.1007/978-1-4020-6356-5

15. Coetzee, E., Krauskopf, B., and Lowenberg, M. H. "The Dynamical Systems Toolbox: Integrating AUTO into Matlab", *16th US National Congress of Theoretical and Applied Mechanics*, Pennsylvania State University Paper USNCTAM2010-827, 2010.

16. Doedel, E. J. "*AUTO-07P, Continuation and Bifurcation Software for Ordinary Differential Equations, Ver. 07P*", http://www.macs.hw.ac.uk/~gabriel/auto07/auto.html [retrieved 11 October 2020].

17. Klyde, D. H., and Mitchell, D. G. "Investigating The Role of Rate Limiting in Pilot-Induced Oscillations", *Journal of Guidance, Control, and Dynamics,* Vol. 27, No. 5, 2004, pp. 804-813.
doi: 10.2514/1.3215

18. Alcalá, I., Gordillo, F., and Aracil, J. "Saddle-Node Bifurcation of Limit Cycles in a Feedback System with Rate Limiter", *2001 European Control Conference (ECC)*, Paper 354-359, 2001.
doi: 10.23919/ECC.2001.7075932

19. Ortega, M. G., Aracil, J., Gordillo, F., and Rubio, F. R. "Bifurcation analysis of a feedback system with dead zone and saturation", *IEEE Control Systems Magazine,* Vol. 20, No. 4, 2000, pp. 91-101.
doi: 10.1109/37.856182

20. Duda, H. "Prediction of Pilot-in-the-Loop Oscillations Due to Rate Saturation", *Journal of Guidance, Control, and Dynamics*, Vol. 20, No. 3, 1997, pp. 581-587.
doi: 10.2514/2.4080

21. Sørensen, C. B., Mosekilde, E., and Gránásy, P. "Nonlinear dynamics of a vectored thrust aircraft", *Physica Scripta*, Vol. T67, 1996, pp. 176-183.
doi: 10.1088/0031-8949/1996/t67/034

22. Duda, H. "Effects of rate limiting elements in flight control systems - A new PIO-criterion", *Guidance, Navigation, and Control Conference*, AIAA Paper 95-3204-CP, 1995.
doi: 10.2514/6.1995-3204

23. Merlin, P. W. "Free Enterprise: Contributions of the Approach and Landing Test (ALT) Program to the Development of the Space Shuttle Orbiter", *Space 2006*, AIAA Paper 2006-7467, 2006.
doi: 10.2514/6.2006-7467

24. Smith, J. W. "Analysis of a longitudinal pilot-induced oscillation experienced on the approach and landing test of the space shuttle," *NASA Technical Memorandum 81366*. National Aeronautics and Space Administration, Ames Research Center, Edwards, CA, 1981.

25. Smith, J. W., and Edwards, J. W. "Design of a Nonlinear Adaptive Filter for Suppression of Shuttle Pilot-Induced Oscillation Tendencies," *NASA Technical Memorandum 81349*. Edwards, California, 1980.

26. McRuer, D. T., *Aviation Safety and Pilot Control: Understanding and Preventing Unfavorable Pilot-Vehicle Interactions*, chapter 2, The National Academies Press, Washington, DC, 1997.
doi: 10.17226/5469

27. Fielding, C., and Flux, P. K. "Non-linearities in flight control systems", *The Aeronautical Journal*, Vol. 107, No. 1077, 2003, pp. 673-686.
doi: 10.1017/S0001924000013543